International Journal of Nanomedicine

Dovepress
open access to scientific and medical research

Open Access Full Text Article

ORIGINAL RESEARCH

Fe_3O_4-based PLGA nanoparticles as MR contrast agents for the detection of thrombosis

This article was published in the following Dove Press journal:
International Journal of Nanomedicine
9 February 2017
Number of times this article has been viewed

Jia Liu[1]
Jie Xu[1]
Jun Zhou[1]
Yu Zhang[1]
Dajing Guo[1]
Zhigang Wang[2]

[1]Department of Radiology, [2]Department of Ultrasound, Institute of Ultrasound Imaging, The Second Affiliated Hospital of Chongqing Medical University, Yuzhong, Chongqing, People's Republic of China

Abstract: Thrombotic disease is a great threat to human health, and early detection is particularly important. Magnetic resonance (MR) molecular imaging provides noninvasive imaging with the potential for early disease diagnosis. In this study, we developed Fe_3O_4-based poly(lactic-*co*-glycolic acid) (PLGA) nanoparticles (NPs) surface-modified with a cyclic Arg-Gly-Asp (cRGD) peptide as an MR contrast agent for the detection of thrombosis. The physical and chemical characteristics, biological toxicity, ability to target thrombi, and biodistribution of the NPs were studied. The Fe_3O_4-PLGA-cRGD NPs were constructed successfully, and hematologic and pathologic assays indicated no in vivo toxicity of the NPs. In a rat model of $FeCl_3$-induced abdominal aorta thrombosis, the NPs readily and selectively accumulated on the surface of the thrombosis and under vascular endothelial cells ex vivo and in vivo. In the in vivo experiment, the biodistribution of the NPs suggested that the NPs might be internalized by the macrophages of the reticuloendothelial system in the liver and the spleen. The T2 signal decreased at the mural thrombus 10 min after injection and then gradually increased until 50 min. These results suggest that the NPs are suitable for in vivo molecular imaging of thrombosis under high shear stress conditions and represent a very promising MR contrast agent for sensitive and specific detection of thrombosis.

Keywords: iron oxide, poly(lactic-*co*-glycolic acid), thrombosis, magnetic resonance imaging, cyclic Arg-Gly-Asp peptide

Introduction

The increasingly high incidence of thromboembolic diseases, such as stroke, myocardial infarction, and pulmonary embolism, threatens human health, and these diseases are major causes of death and disability worldwide.[1,2] The magnitude of this problem is even greater because patients with hypertension, hyperlipidemia, and abnormal glucose metabolism are also predisposed to arterial thrombosis.[3] Early diagnosis of arterial thrombus would allow timely clinical intervention to avoid permanent tissue infarction and reduce morbidity and mortality.

Emerging conventional invasive and noninvasive imaging techniques for thrombus detection, such as computer tomography angiography and digital subtraction angiography, are characterized by relatively poor spatial resolution and cannot visualize specific biological processes in the thrombus. New imaging procedures and strategies for the detection of thrombi are required. Accordingly, targeted probes for molecular imaging are emerging as powerful tools in cardiovascular medicine for thrombus detection with high sensitivity and specificity. A variety of particles have been reported in the literature for thrombosis detection.[4–17] Compared with ultrasound,[4–8] nuclear medicine,[9,10,18] and computed tomography (CT),[11] the advantages of magnetic resonance imaging (MRI) that are particularly relevant in the context of cardiovascular diseases are its high temporal and spatial imaging resolution, high soft tissue contrast,

Correspondence: Dajing Guo
Department of Radiology, The Second Affiliated Hospital of Chongqing Medical University, No 74 Linjiang Rd, Yuzhong District, 400010 Chongqing, People's Republic of China
Tel +86 23 6369 3781
Email guodaj@163.com

submit your manuscript | www.dovepress.com
Dovepress
http://dx.doi.org/10.2147/IJN.S123228

and ability to display thrombus morphology, physiology, and molecular events using a single imaging modality. Specific molecular MR probes enable the visualization of molecular and cellular processes. Additionally, molecular MR probes allow the characterization and visualization of early changes in disease and thus can improve the planning of therapeutic regimens and monitoring of disease.

With the continued development of contrast agents and MRI sequences, there is great hope that molecular MRI can improve the diagnosis of thrombosis. In recent years, MR contrast agents, such as gadolinium diethylenetriaminepentaacetic acid (Gd-DTPA), superparamagnetic iron oxide (SPIO), and ultra-small superparamagnetic particles of iron oxide (USPIOs), have been successfully encapsulated into macromolecular polymer particles to create novel contrast agents.[12–17] The fibrin-targeted MR molecular probe EP-2104R has entered clinical trials with encouraging results.[19] Comparatively Gd-DTPA, SPIO and USPIO have the advantages of long half-lives, high relaxation rates, and minimal side effects.[20,21] Most previous studies of thrombosis detection molecules have focused on their physicochemical properties in vitro and targeting abilities in vivo.[12,15] In some studies, new MRI contrast agents targeting activated platelets have been successfully prepared and used to detect endovascular thrombi in vivo.[17,22,23] Similarly, in our previous studies, we synthesized novel types of thrombus-targeting particles and confirmed their targeting ability and contrast-enhancing effects in vitro.[24,25] Although further validation of their targeting ability, biodistribution, and toxicity in vivo are required, there have been few studies of MRI contrast agent behavior, particularly in vivo, which limits their potential translation to clinical use.

In this study, we will focus on the in vivo properties of nanoparticles (NPs), including their drug distribution, biological toxicity, and targeting ability that must be established prior to translation to the clinical applications. First, to increase their targeting ability, a cyclic Arg-Gly-Asp (cRGD) peptide was used in this study instead of the Arg-Gly-Asp-Ser (RGDS) peptide. In addition, the constructed particles were smaller than those in our previous studies[24,25] to prevent the accumulation of the majority of NPs in the liver and spleen. Furthermore, we dynamically visualized the targeting procedures by 7.0-T MRI using an abdominal aorta model of thrombosis in rats because of its possible application to the more complicated in vivo situation.

Materials and methods

Materials

Poly(lactic-*co*-glycolic acid) (PLGA; containing 75% lactide and 25% glycolide, with a molecular weight of 12,000, end group = COOH) was purchased from Jinan Daigang Biological Material Co., Ltd. (Shangdong, China). Iron oxide NPs that had been surface-modified with oleic acid (Fe_3O_4) were provided by Ocean Nano Technology Co., Ltd. (Springdale, AR, USA). The cRGD peptide was synthesized by GL Biochem (Shanghai, China). Polyvinyl alcohol (PVA) with an average molecular weight of 30,000–70,000, 2-(*N*-morpholino) ethanesulfonic acid (MES), *N*-hydroxysuccinimide (NHS), and 1-ethyl-3-(3-dimethylaminopropyl) carbodiimide hydrochloride (EDC) were purchased from Sigma-Aldrich Corporation (St Louis, MO, USA). All other reagents used were of at least analytical grade.

Preparation and physical and chemical characterization of the NPs

Fe_3O_4-based PLGA NPs were prepared using the W/O/W method, which was modified based on reports in the literature.[24–27] PLGA was used as the core of the drug carrier, Fe_3O_4 was embedded in the layer of PLGA, and cRGD was coated on the surface of the PLGA-Fe_3O_4 layer. A schematic representation of the Fe_3O_4-PLGA-cRGD NPs is shown in Figure 1.

PLGA (50 mg) and Fe_3O_4 (24 μL of a 25 mg/mL solution) were fully dissolved in 1 mL of dichloromethane as the oil phase, and 0.2 mL of double-distilled water and 5 mL of 4% PVA solution served as the inner and outer aqueous phases, respectively. An ultrasonic oscillation instrument was used twice to apply acoustic vibrations for 60 s each time to produce a double-emulsion solution. The remaining steps in the production of PLGA-Fe_3O_4 NPs were identical to those in our previous study.[25] Fe_3O_4-PLGA-cRGD was prepared using carbodiimide-mediated amide bond formation. First, appropriate amounts of EDC and NHS were added at a molar ratio of 1.5:1–0.1 M MES buffer solution (pH 6) to activate the carboxyl of Fe_3O_4-PLGA. Second, 0.1 M MES buffer solution (pH 8) was dissolved again, after centrifugation and washing, and then 10 mg of cRGD peptide was added and allowed to react for 24 h at 4°C. Finally, the Fe_3O_4-PLGA-cRGD was rinsed with double-distilled water to remove the unreacted materials and air-dried at room temperature.

After an appropriate amount of NPs was suspended in double-distilled water, the morphology, surfaces, and dispersion of the NPs were observed with an optical microscope, and the internal structures were observed with a transmission electron microscope. The attachment of cRGD onto the PLGA NPs was confirmed using laser scanning confocal microscopy. The cRGD was labeled with fluorescein isothiocyanate (FITC). The sizes, zeta potentials, and polydispersity indices (PDIs) of the different NPs were determined at 25°C

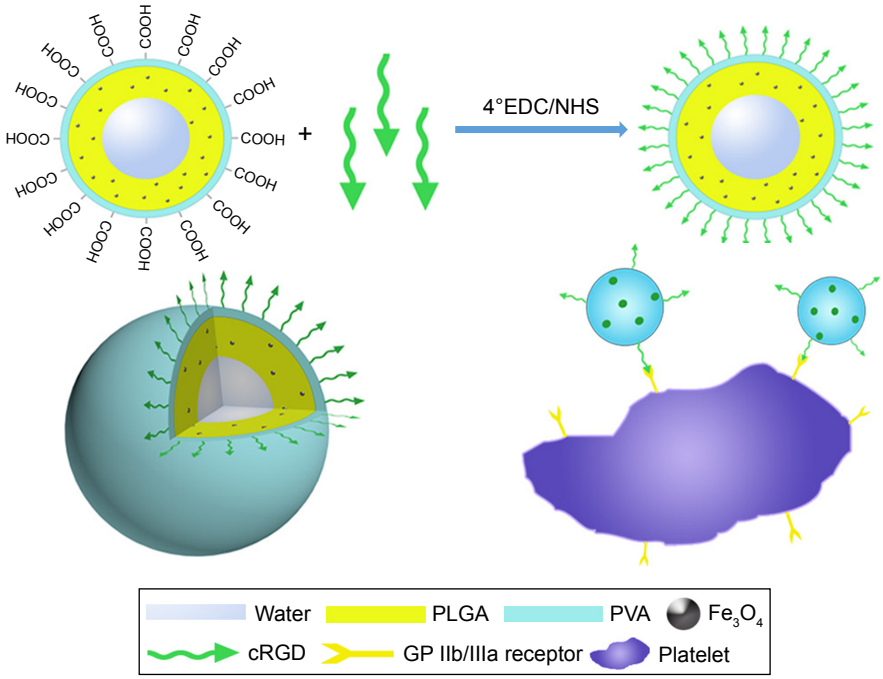

Figure 1 Schematic representation of Fe_3O_4-PLGA-cRGD nanoparticles.
Abbreviations: cRGD, cyclic Arg-Gly-Asp; EDC, 1-ethyl-3-(3-dimethylaminopropyl) carbodiimide hydrochloride; GP IIb/IIIa, glycoprotein IIb/IIIa; NHS, *N*-hydroxysuccinimide; PLGA, poly(lactic-*co*-glycolic acid); PVA, polyvinyl alcohol.

using a laser particle size analyzer. The carrier rate of cRGD was measured using flow cytometry. The iron concentration was measured by atomic absorption spectrometry. All instruments and measurements were provided in the "Methods" section of our previous study.[25]

In vivo toxicity study

Sprague Dawley (SD) rats weighing between 200 and 230 g each were purchased from the Animal Center of Chongqing Medical University. The animal experiments were approved by the Animal Ethics Committee of Chongqing Medical University and conducted in accordance with the guidelines of the Institutional Animal Care and Use Committee of Chongqing Medical University.

Eight SD rats were used for the in vivo toxicity study. These rats were raised in stainless cages in ventilated animal rooms with a typical environment (23°C±1°C, 55%±15% humidity, and 12 h light/dark cycle) and had free access to water and food. After acclimatization to the environment, the rats were separated into two groups (n=4). Then, Fe_3O_4-PLGA or Fe_3O_4-PLGA-cRGD NPs at a final dosage of 1 mg lyophilized powder dissolving 1 mL phosphate-buffered saline (PBS) was administered to the rats by tail vein injection. Body weights were recorded every morning, and overall animal health was determined by careful observations for signs of irritation, pain, discomfort, and inflammation.

Rat blood samples (1.0 mL) were obtained from the retinal vein before and 1, 3, and 24 h and 3 and 7 d after injection of the Fe_3O_4-based PLGA NPs for the analysis of serum glutamic pyruvic transaminase (GPT), glutamic oxaloacetic transaminase (GOT), total bilirubin, creatinine, and urea. The influence of the NPs on hepatic and kidney function and hematologic indices were evaluated based on blood biochemical parameters analyzed by a Catalyst Dx™ (Idexx, Maine, ME, USA) and a Mindray BC-2800Vet (Mindray, Shenzhen, China).

Then, the rats were dissected, and major organs, such as the heart, liver, spleen, lungs, and kidney, were harvested, rinsed with PBS and embedded in a paraffin for hematoxylin and eosin (H&E) staining and pathologic evaluation.

Abdominal aorta model of wall-adherent thrombosis

In vivo thrombi were induced by $FeCl_3$ injury to the abdominal aorta. Before the experiment, the rats were anesthetized intraperitoneally with pentobarbital sodium (35 mg/kg). The entire process was described in the "Methods" section of our previous study.[25]

MRI scans were performed on the SD rats before and after the abdominal aorta model of wall-adherent thrombosis was successfully achieved at 30 min using a 7.0-T MR microimaging system (BioSpec 70/20USR, Bruker, Ettlingen, Germany) with a rat experiment coil (Transmit/receive 2-channel rat body, Bruker). Axial T2-weighted

imaging (T2WI) at the thrombosis site was performed using the TurboRARE sequence with the following parameters: TR =1,400 ms, TE =25 ms, FA =90°, NEX =8, FOV =60 mm, matrix =256×256, and slice thickness =1 mm. MR angiography scanning followed using a 3D flash sequence with the following parameters: TR =15 ms, TE =2.7 ms, FA =20°, NEX =2, FOV =60 mm, matrix =256×256, and slice thickness=17 mm. During the MRI scanning process, the animals were connected to a breathing-rate monitor, and anesthesia was continuously provided with 0.2% isoflurane and a breathing rate maintained at 48 breaths per minute.

When the in vivo MRI scans were complete, the animals were deeply anesthetized with an appropriate dose of pentobarbital sodium. Transcardiac perfusion with saline was performed through the left ventricle. Then, the injured abdominal aortas were removed and embedded in paraffin for H&E staining to observe the thrombus using an optical microscope.

Ex vivo study of targeting ability

After the abdominal aorta model of wall-adherent thrombosis was successfully achieved at 30 min, the injured abdominal aortas were removed, the Fe_3O_4-PLGA NPs or the Fe_3O_4-PLGA-cRGD NP solution was injected through one end of the ex vivo thrombosis, and frozen sections were cut for H&E staining after washing it with saline for 5 min. All pathologic samples were examined by an experienced pathologist who was blinded to the grouping.

In vivo MRI

Measurement of NP distribution

Eight SD rats were consecutively and randomly divided into two groups, the Fe_3O_4-PLGA NP group and the Fe_3O_4-PLGA-cRGD NP group. MRI scans were performed on the SD rats before and after $FeCl_3$ injury to the abdominal aorta and at 0 min, 10 min, 20 min, 30 min, 1 h, 2 h, and 3 h after injection of the NPs. Coronal T2-weighted images were acquired using the same TurboRARE sequence as described in the previous section. The signal intensities (SIs) of the liver, spleen, kidney, and muscle of rats were obtained at relatively homogeneous regions of interest (ROI) with the same diameters in the same slice of T2-weighted images at each time point after intravenous injection of 1 mL of PBS containing 1 mg of a lyophilized powder of either Fe_3O_4-PLGA or Fe_3O_4-PLGA-cRGD NPs. The signal-to-noise ratios (SNRs) were plotted against time. The SNRs were calculated using the following formula: SNRs = SI (liver, spleen, or kidney)/SI (muscle).

Thrombus targeting

Eight SD rats were consecutively and randomly divided into two groups, the Fe_3O_4-PLGA NP group and the Fe_3O_4-PLGA-cRGD NP group. MRI scans were performed on the SD rats before and after $FeCl_3$ injury to the abdominal aorta and at 0, 10, 20, 30, 40, and 50 min after injection of NPs, and axial T2-weighted images of the thrombus were obtained using the same parameters of the TurboRARE sequence as described in the previous section. When the in vivo MRI scans were finished, the injured abdominal aortas were removed and frozen pathology sections were cut for H&E staining, to observe the targeting ability of the NPs at the thrombus.

Statistical analysis

The data were analyzed using Statistical Program for the Social Sciences (SPSS for Windows, version 19.00, Chicago, IL, USA). The continuous variables are presented as mean ± standard deviation and the categorical variables are reported numerically and in percentages. Two-way analysis of variance was used to compare the differences between the SNRs of the two groups at each time point for the liver, spleen, and kidney. Independent sample *t*-tests were used to compare the average diameter of the NPs between the two groups. Statistical significance was defined at $P<0.05$.

Results

Characteristics of the Fe_3O_4-based PLGA NPs

Optical microscopy showed relatively homogeneous particle sizes among the NPs, with spherical, smooth surfaces, and good dispersion (Figure 2). The iron oxide particles were relatively uniformly distributed in the NP shells (Figure 3). Confocal laser microscopy showed that cRGD labeled with FITC was successfully coated onto the surface of the PLGA NPs (Figure 4). The average particle diameters, PDIs, zeta potentials, and carrier rates of the NPs for Fe_3O_4 and cRGD are shown in Table 1.

In vivo toxicity of different NPs in rats

No mortality was observed throughout the entire 7-day study. The body weights of the SD rats remained constant. In the hematologic and biochemical assays, there were no significant differences between the two groups. With respect to liver and kidney function, GPT and GOT increased slightly within 1 and 3 h, but returned to normal at the 24 h, 3 d, and 7 d time points after injection in the two groups (Table 2). However, there was no obvious abnormality in blood composition (Table 3). The heart, liver, spleen, lungs, and kidneys were harvested for H&E staining 7 d postinjection. No evidence of inflammatory reactions or necrosis was observed in the two groups, and no abnormal cell morphology was detected (Figure 5).

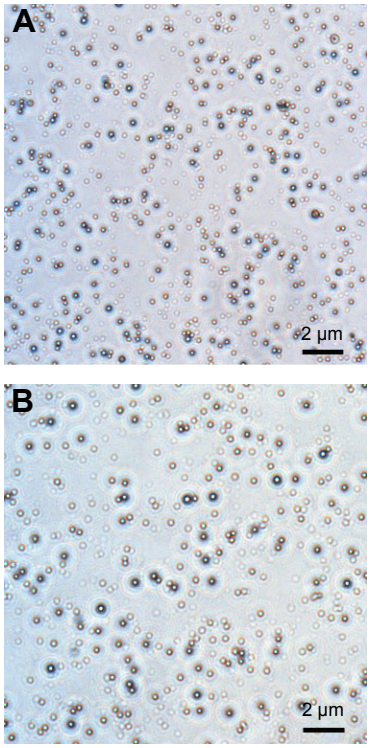

Figure 2 Optical microscopic images (600×).
Notes: (**A**) Fe_3O_4-PLGA NPs and (**B**) Fe_3O_4-PLGA-cRGD NPs. The NPs had a regular shape and were relatively uniform in size.
Abbreviations: cRGD, cyclic Arg-Gly-Asp; NPs, nanoparticles; PLGA, poly(lactic-*co*-glycolic acid).

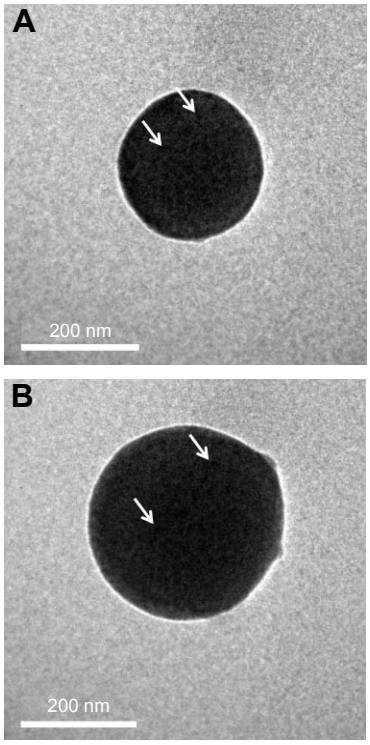

Figure 3 Transmission electron microscopic images.
Notes: (**A**) Fe_3O_4-PLGA NPs and (**B**) Fe_3O_4-PLGA-cRGD nanoparticles. The iron oxide particles (white arrows) exhibited a relatively uniform distribution on the nanosized, spherical shell.
Abbreviations: cRGD, cyclic Arg-Gly-Asp; PLGA, poly(lactic-*co*-glycolic acid).

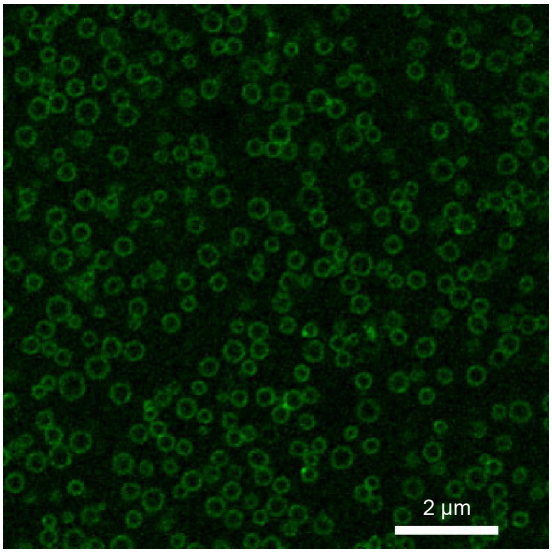

Figure 4 Laser scanning confocal microscopic image of the Fe_3O_4-PLGA-cRGD NPs.
Note: Annular green fluorescence was observed around NPs, but almost no fluorescence was detected in the inner aqueous phase.
Abbreviations: cRGD, cyclic Arg-Gly-Asp; NPs, nanoparticles; PLGA, poly(lactic-*co*-glycolic acid).

Ex vivo thrombosis-targeting ability

The abdominal aorta model of wall-adherent thrombosis was successfully constructed without any side effects in rats; in vivo MRI scans showed that a thrombus formed in each rat abdominal aorta, as corroborated by pathologic examination (Figure 6). In the ex vivo targeting experiment, frozen pathologic sections revealed dense binding of Fe_3O_4-PLGA-cRGD NPs on the surface of the thrombus and under vascular endothelial cells, but no Fe_3O_4-PLGA NPs were observed on the surface of the thrombus, and only spare NPs were found under vascular endothelial cells (Figure 7).

NP distribution in vivo

The SNRs of the liver, spleen, and kidney before and at each time point after intravenous injection of different NPs are shown in Figure 8. After the injection of these NPs, the SNRs of both the liver and the spleen decreased significantly at 10 min. The SNRs of the liver decreased

Table 1 Characteristics of Fe_3O_4-based PLGA NPs

	Fe_3O_4-PLGA	Fe_3O_4-PLGA-cRGD
Size (nm)	289.5±7.4	368.2±4.5
Polydispersity index	0.077±0.031	0.081±0.058
Zeta potential (mV)	−7.53±0.71	−9.43±0.86
Carrier rate of Fe_3O_4 (%)	66.02±1.7	64.67±0.9
Carrier rate of cRGD (%)	–	99.93±0.06

Note: The Fe_3O_4-PLGA-cRGD NPs are larger than the Fe_3O_4-PLGA NPs ($P<0.05$).
Abbreviations: cRGD, cyclic Arg-Gly-Asp; NPs, nanoparticles; PLGA, poly(lactic-*co*-glycolic acid).

Table 2 Blood chemistry parameters of rats injected with Fe_3O_4-based PLGA nanoparticles

	1 h	3 h	24 h	3 d	7 d
GPT (20–61 U/L)*					
Fe_3O_4-PLGA	65.50±2.64**	65.50±3.32**	45.50±3.11	47.50±12.4	44.70±14.86
Fe_3O_4-PLGA-cRGD	64.50±2.65**	65.75±4.92**	44.74±2.06	47.75±13.37	47.25±11.53
GOT (39–111 U/L)*					
Fe_3O_4-PLGA	132.00±14.24**	122.70±22.29**	94.50±16.98	93.50±14.48	89.00±11.05
Fe_3O_4-PLGA-cRGD	122.50±8.02**	117.00±14.49**	92.50±15.55	95.50±13.20	88.00±10.86
Total bilirubin (2–12 μmol/L)*					
Fe_3O_4-PLGA	4.50±1.29	3.50±1.29	4.50±1.29	4.25±1.50	4.50±1.29
Fe_3O_4-PLGA-cRGD	3.50±0.58	4.25±1.25	4.00±1.41	4.25±1.50	3.75±0.96
Creatinine (4–57 μmol/L)*					
Fe_3O_4-PLGA	33.75±3.10	30.75±5.32	30.25±3.30	32.50±4.92	37.00±11.66
Fe_3O_4-PLGA-cRGD	34.25±1.50	33.25±5.56	33.25±3.77	34.75±4.57	37.00±6.73
Urea (3.2–7.5 mmol/L)*					
Fe_3O_4-PLGA	5.75±0.96	6.42±0.90	4.50±1.15	5.45±1.62	6.92±0.46
Fe_3O_4-PLGA-cRGD	6.00±0.60	5.98±0.67	5.55±0.86	5.85±1.14	6.43±0.72

Notes: *The remaining indicators are within normal ranges. **GPT and GOT increased slightly within 1 and 3 h, but returned to normal at the 24 h, 3 d, and 7 d time points after injection in the two groups.
Abbreviations: cRGD, cyclic Arg-Gly-Asp; GPT, glutamic pyruvic transaminase; GOT, glutamic oxaloacetic transaminase; PLGA, poly(lactic-*co*-glycolic acid).

to their lowest level at 30 min and then increased slightly at 1 h. The SNRs of the spleen decreased to their lowest level at 1 h and increased slightly at 2 h. The SNRs of the liver and spleen were still lower than before injection at 3 h. The SNRs of the kidneys were slightly lower at 1 h and remained low for 2 h, with only a slight change. There were no significant differences in the SNRs of the liver, spleen, and kidney between the two groups at each time point ($P<0.05$).

In vivo MRI of the targeted thrombus

In both groups, preinjection MRI permitted clear identification of the abdominal aorta based on the bright blood signal inside the vessel. After intravenous injection in the

Table 3 Blood composition of the Fe_3O_4-based PLGA nanoparticle group

	1 h	3 h	24 h	3 d	7 d
White blood cells (2.9–15.3×10⁹/L)#					
Fe_3O_4-PLGA	6.55±1.30	5.98±1.77	5.15±1.42	5.70±1.69	5.83±1.37
Fe_3O_4-PLGA-cRGD	7.43±1.73	6.48±1.81	4.25±1.08	5.68±1.53	4.93±1.16
Monocytes (0.0–0.5×10⁹/L)#					
Fe_3O_4-PLGA	0.15±0.06	0.20±0.82	0.23±0.13	0.18±0.10	0.20±0.08
Fe_3O_4-PLGA-cRGD	0.18±0.10	0.18±0.10	0.20±0.82	0.30±0.82	0.28±0.10
Lymphocytes (2.6–13.5×10⁹/L)#					
Fe_3O_4-PLGA	4.28±0.57	5.20±1.78	4.18±1.05	4.50±0.73	3.80±0.96
Fe_3O_4-PLGA-cRGD	4.53±0.81	3.50±0.79	3.88±0.77	4.28±0.67	4.80±0.77
Neutrophils (0.4–3.2×10⁹/L)#					
Fe_3O_4-PLGA	2.28±0.46	2.10±0.91	1.78±0.65	1.60±0.43	2.33±0.71
Fe_3O_4-PLGA-cRGD	2.55±0.56	2.08±0.83	2.18±0.44	2.28±0.78	1.78±0.57
Red blood cells (5.6–7.89×10¹²/L)#					
Fe_3O_4-PLGA	7.33±0.42	6.88±0.37	6.99±0.49	6.91±0.49	6.66±0.67
Fe_3O_4-PLGA-cRGD	6.64±0.69	6.56±0.77	6.49±0.66	6.78±0.71	6.93±0.32
Hemoglobin (120–150 g/L)#					
Fe_3O_4-PLGA	136.00±10.03	139.00±6.58	139.00±4.83	134.50±8.27	138.75±5.44
Fe_3O_4-PLGA-cRGD	138.00±8.08	141.50±5.20	139.25±7.76	131.75±5.68	136.75±5.56
Platelets (100–1,610×10⁹/L)#					
Fe_3O_4-PLGA	775.25±144.9	765.00±46.44	924.00±174.86	787.00±121.2	853.50±66.00
Fe_3O_4-PLGA-cRGD	863.25±116.69	701.00±120.8	922.00±235.18	748.50±52.26	833.75±178.18

Note: #Normal range.
Abbreviations: cRGD, cyclic Arg-Gly-Asp; PLGA, poly(lactic-*co*-glycolic acid).

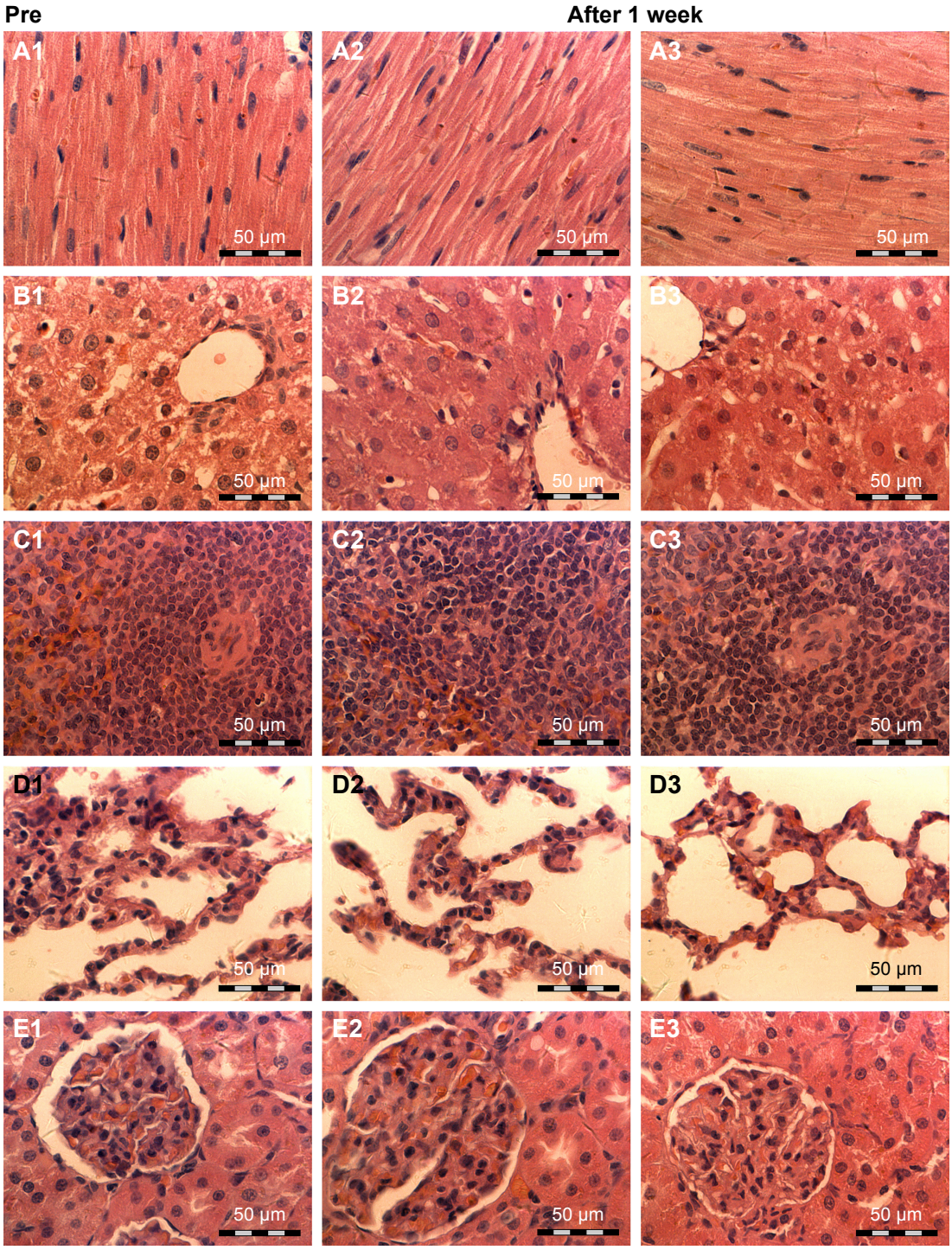

Figure 5 Pathologic hematoxylin and eosin staining (**A**–**E**) of the heart, liver, spleen, lung, and kidney. (A1–E1) before NP injection, (A2–E2) after injection of Fe_3O_4-PLGA NPs, and (A3–E3) after injection of Fe_3O_4-PLGA-cRGD NPs. There was no evidence of inflammatory reactions or necrosis in the two groups, and no abnormal cell morphology was found. The magnification is 400×.
Abbreviations: cRGD, cyclic Arg-Gly-Asp; NPs, nanoparticles; PLGA, poly(lactic-*co*-glycolic acid).

Fe_3O_4-PLGA-cRGD NP group, the T2 signal decreased at the mural thrombus at 10 min. The signal of the peripheral zones of the abdominal aorta clearly decreased and then gradually increased until 50 min. There was no significant decrease in the signal of the abdominal aorta before and after injection in the Fe_3O_4-PLGA NP group (Figure 9). H&E staining of frozen sections showed that a few of the Fe_3O_4-PLGA-cRGD NPs had gathered on the surface of the thrombus and that there were many NPs under vascular endothelial cells; no NPs were found in the sample injected with Fe_3O_4-PLGA NPs (Figure 10).

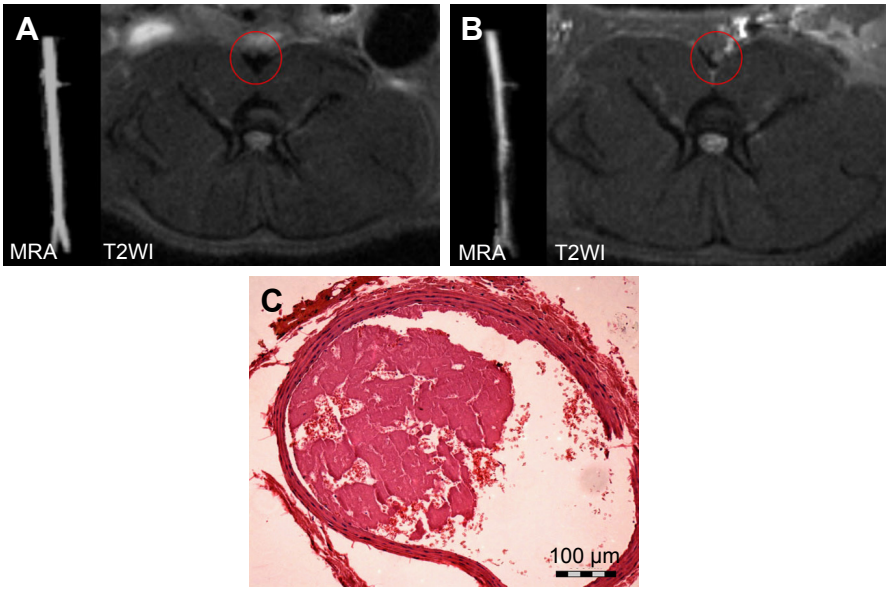

Figure 6 MRA, magnetic resonance imaging T2WI axial images, and pathologic H&E staining of the abdominal aorta.
Notes: (**A**) Before induction of the thrombosis model, (**B**) post-induction, and (**C**) H&E staining of a section of the model. MRA revealed vessel lumen narrowing after the $FeCl_3$-induced model was successfully constructed, and the signal in the abdominal aorta changed from low to high on the T2WI axial image. H&E staining confirmed that the mural thrombus was mixed. The magnification is 100×.
Abbreviations: H&E, hematoxylin and eosin; MRA, magnetic resonance angiography; T2WI, T2-weighted imaging.

Discussion

PLGA has emerged as an important biocompatible and nontoxic polymer with numerous applications in drug delivery, medical, and tissue engineering and surgical devices due to its biocompatibility, biodegradability, and sustained-release properties.[28–31] In recent years, with the advent of block copolymers, the use of PLGA in the development of controlled and targeted drug delivery systems has substantially increased.[32] The attractive features of PLGA-based NPs, such as their small size, high structural integrity, stability, ease of fabrication, tunable properties, controlled-release capabilities, and surface functionalization characteristics, make them versatile therapeutic delivery vehicles. In this study, Fe_3O_4 was embedded in the PLGA shell, and cRGD was linked to the surface of PLGA to synthesize Fe_3O_4-PLGA-cRGD NPs for the detection of thrombosis. The PLGA NPs showed relatively homogeneous particle sizes, with spherical, smooth surfaces, and good dispersion. No aggregation was observed during and after the preparation of the PLGA NPs. After the conjugation of

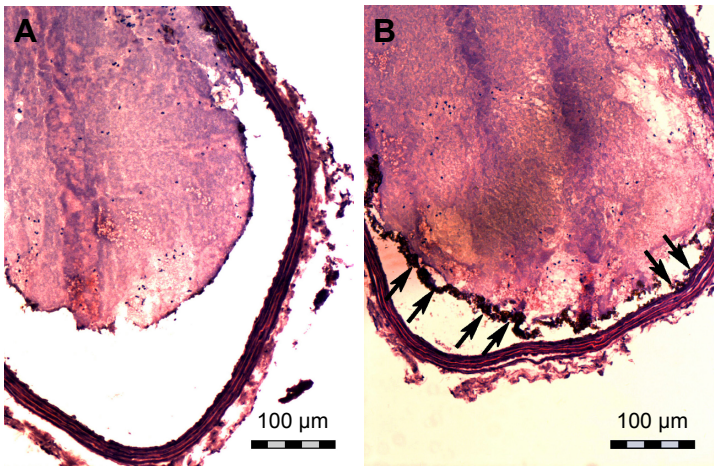

Figure 7 Hematoxylin and eosin staining of frozen sections of the ex vivo thrombus after injection of the NPs.
Notes: (**A**) Fe_3O_4-PLGA NPs and (**B**) Fe_3O_4-PLGA-cRGD NPs. Many of the Fe_3O_4-PLGA-cRGD NPs gathered on the surface of the thrombus (black arrows), and no NPs were found on the surface of the thrombus in the sample with Fe_3O_4-PLGA NPs. The magnification is 200×.
Abbreviations: cRGD, cyclic Arg-Gly-Asp; NPs, nanoparticles; PLGA, poly(lactic-*co*-glycolic acid).

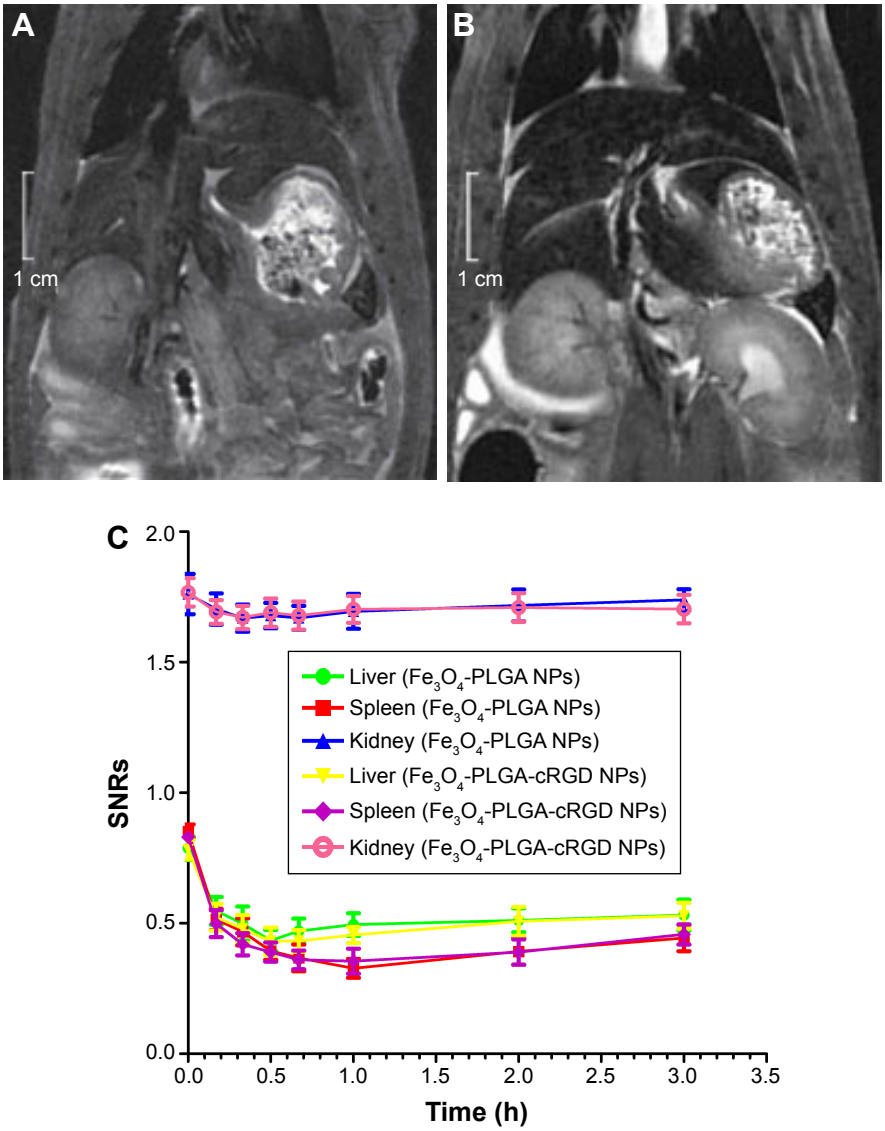

Figure 8 MRI T2WI images of the abdomen and graph of SNRs.
Notes: (**A**) Before injection of the Fe_3O_4-PLGA-cRGD NPs. (**B**) After injection of the Fe_3O_4-PLGA-cRGD NPs at 30 min. (**C**) SNRs curves of the liver, spleen, and kidneys before and after the injection of Fe_3O_4-PLGA and Fe_3O_4-PLGA-cRGD NPs. MRI T2WI images of the abdomen demonstrated that the signals in the liver and spleen decreased significantly after NP injection. The SNRs of both the liver and spleen decreased significantly after NP injection as well, and the SNRs of the kidney decreased slightly.
Abbreviations: cRGD, cyclic Arg-Gly-Asp; MRI, magnetic resonance imaging; NPs, nanoparticles; PLGA, poly(lactic-*co*-glycolic acid); SNRs, signal-to-noise ratios; T2WI, T2-weighted imaging.

cRGD, the Fe_3O_4-PLGA-cRGD NPs were slightly larger than the Fe_3O_4-PLGA NPs. These NPs were safe when injected into the body due to their small size of $<$500 nm, which prevents blockage of blood vessels. In addition, in the in vivo experiment no SD rats died of embolism. Furthermore, given the relatively small particle size of the NPs, we expected the contrast agent to diffuse inside the thrombus, thereby increasing the relative volume of enhancement in a given voxel.

Platelets are the key to thrombus formation and play a role in the development of atherosclerosis. Noninvasive imaging of activated platelets would be of great clinical interest. The abundance of glycoprotein (GP) IIb/IIIa and its change in conformation upon platelet activation make this receptor a unique, highly specific target for imaging.[33,34] The main strategies for NP-targeting delivery utilize either antibodies or peptides. Although monoclonal antibodies have been widely used in the past because of their high affinity, they are limited by their large size and random orientation upon conjugation.[35] Peptides have emerged as an attractive alternative to antibodies due to their smaller size, lower cost, lower immunogenicity, easier production, and long-term stability.[36] RGD peptides, which exist in either linear or cyclic spatial conformations, are small peptides that have been identified

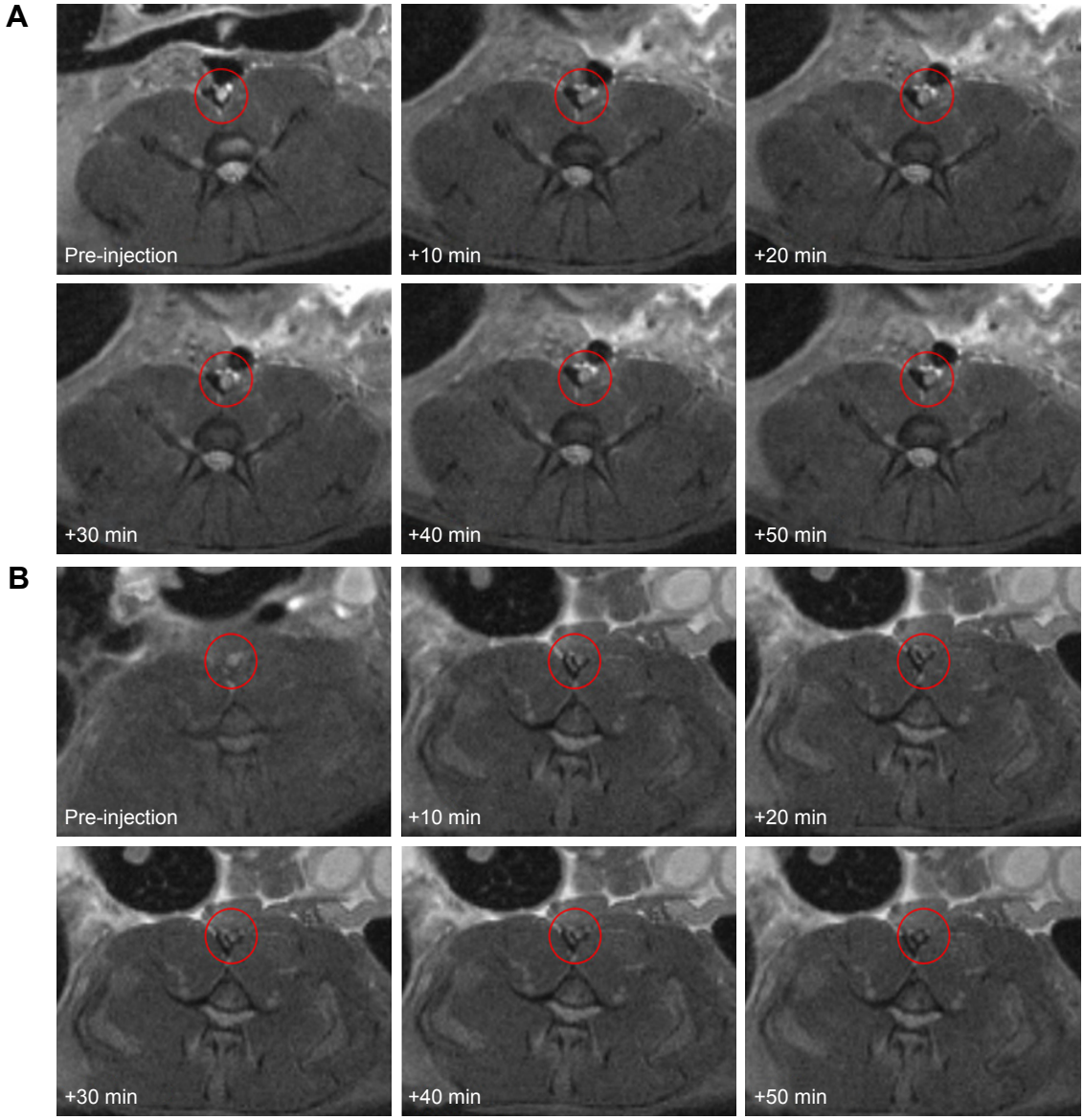

Figure 9 Magnetic resonance imaging T2WI images of the in vivo thrombosis before and after the injection of NPs.
Notes: (**A**) Fe_3O_4-PLGA NPs and (**B**) Fe_3O_4-PLGA-cRGD NPs. Ten minutes after injection, the hyperintense signal of the abdominal aorta began to decrease and the signal of the peripheral zones of the abdominal aorta first obviously decreased and then gradually increased until 50 min in the Fe_3O_4-PLGA-cRGD NP group. There was no significant decrease in the signal of the abdominal aorta before or after injection in the Fe_3O_4-PLGA NP group.
Abbreviations: cRGD, cyclic Arg-Gly-Asp; NPs, nanoparticles; PLGA, poly(lactic-*co*-glycolic acid); T2WI, T2-weighted imaging.

through screening and are effective for molecular imaging of platelets. There is a consensus that the binding affinity of cRGD for GP IIb/IIIa is much greater than that of linear RGD. Furthermore, cRGD appears to be 30-fold more stable[33] displays great affinity for activated platelets under high fluid shear stress.[8] Therefore, in this study, cRGD was conjugated to the surface of PLGA NPs using dicyclohexylcarbodiimide chemistry for the detection of thrombosis in large arteries under high shear flow conditions.

Confocal laser microscopy showed that cRGD labeled with FITC was successfully conjugated to the surface of the PLGA NPs with a carrier rate of 99.93%. According to Song et al,[34] although the avidity of the targeting ligands conjugated to NPs is critical for targeting specificity, the surface density of ligands on the NPs is a more important factor in determining the multivalent effect of ligand-modified NPs and can dramatically enhance the targeting specificity and efficiency of drug delivery/imaging agents, as successfully verified for tumor imaging and therapy. The ability of Fe_3O_4-PLGA-cRGD NPs to target ex vivo wall-adherent thrombosis was confirmed by pathologic examination, which revealed dense binding of Fe_3O_4-PLGA-cRGD NPs to superficial platelets that had adhered or aggregated on the surface of the thrombus and under

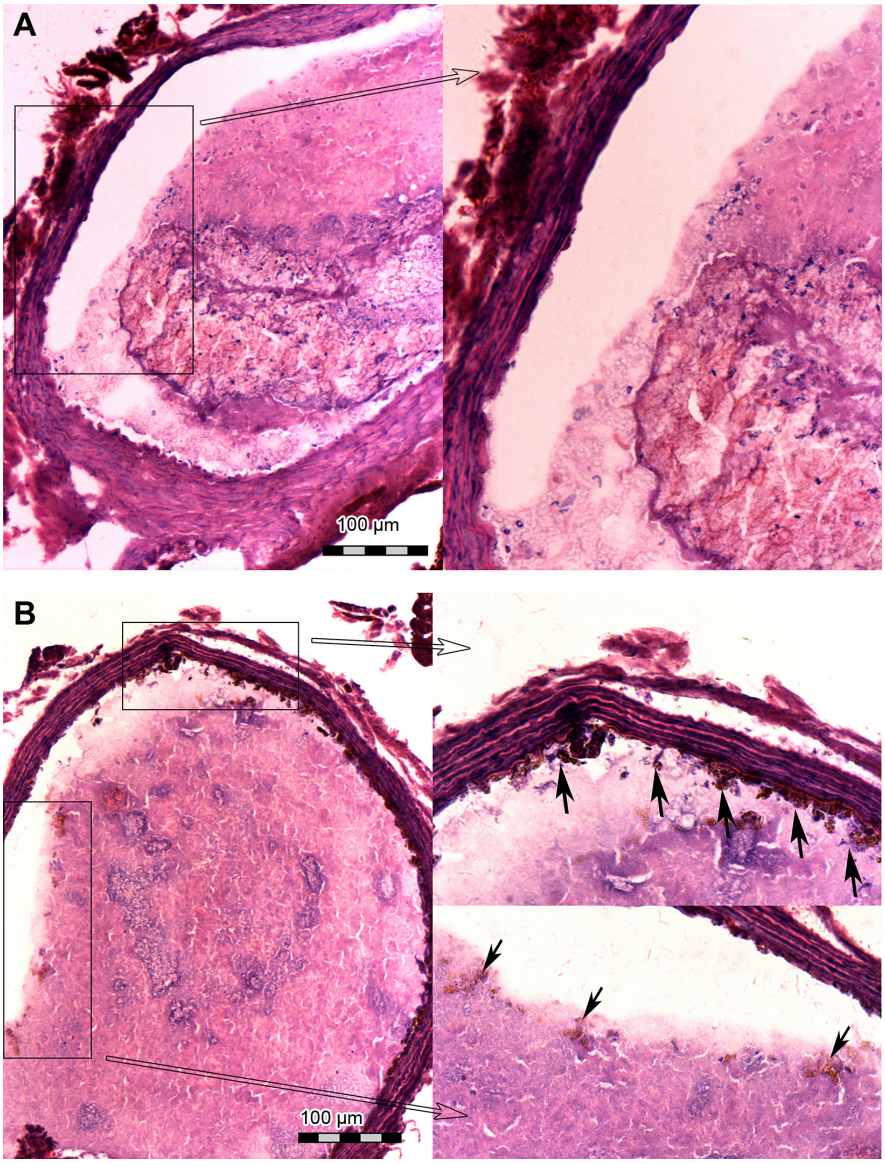

Figure 10 Hematoxylin and eosin staining of frozen sections of thrombi after injection with the NPs after in vivo magnetic resonance imaging scanning was finished.
Notes: (**A**) Fe_3O_4-PLGA NPs and (**B**) Fe_3O_4-PLGA-cRGD NPs. A few of the Fe_3O_4-PLGA-cRGD NPs gathered on the surface of the thrombus, and many NPs were found under vascular endothelial cells (black arrows). No NPs were found in the sample injected with Fe_3O_4-PLGA NPs. These images are magnified ×200.
Abbreviations: cRGD, cyclic Arg-Gly-Asp; NPs, nanoparticles; PLGA, poly(lactic-*co*-glycolic acid).

vascular endothelial cells. However, no Fe_3O_4-PLGA NPs accumulated on the surface of the thrombus, and only sparse binding was observed under vascular endothelial cells. Thrombus formation is initiated by damage to the endothelial lining of blood vessels that exposes the subendothelium to platelets. These platelets adhere to the damaged vessel wall and the surface of the thrombus, thus enabling the aggregation of Fe_3O_4-PLGA-cRGD NPs on superficial platelets as well as on the surface of the thrombus and under vascular endothelial cells.

For in vivo MRI in the thrombus-targeting experiment, to create reproducible semiocclusive platelet-derived thrombosis of the abdominal aorta, we adopted the well-established model of $FeCl_3$-induced thrombosis.[17,37] Importantly, this model guarantees blood circulation and, consequently, flow of the contrast agent over the surface of the wall-adherent thrombus. We demonstrated the utility of Fe_3O_4-PLGA-cRGD NPs as an MR contrast agent for the rapid identification of nonocclusive platelet-containing thrombi in vivo 10 min after injection of the NPs. The T2 signal decreased at the mural thrombus at 10 min, as particularly evident at the peripheral zones of the abdominal aorta, and then gradually increased until 50 min. The effective targeting of the thrombus by Fe_3O_4-PLGA-cRGD NPs provided excellent T2 MR contrast, and the T2 signal decreased over time. After MRI scanning, frozen pathologic sections revealed results similar to those

for the ex vivo wall-adherent thrombosis section. A great quantity of Fe_3O_4-PLGA-cRGD NPs was accumulated on the surface of the thrombus and under vascular endothelial cells, which demonstrated that the Fe_3O_4-PLGA-cRGD NPs had a good ability to target activated platelets ex vivo and in vivo. Conversely, the nonspecific Fe_3O_4-PLGA NPs did not display any persistent signal enhancement and did not specifically enhance the thrombus, as expected.

However, the differences between the ex vivo and in vivo tests should not be underestimated; more Fe_3O_4-PLGA-cRGD NPs were observed in the ex vivo wall-adherent thrombosis section and fewer Fe_3O_4-PLGA-cRGD NPs targeting the thrombosis and impaired vascular endothelium were observed in sections after MRI scanning. These differences in behavior can likely be explained by the high-shear flow conditions in large arteries, which would wash away some of the Fe_3O_4-PLGA-cRGD NPs from the wall-adherent thrombosis. However, a substantial amount of Fe_3O_4-PLGA-cRGD NPs were retained in the abdominal aorta and generated sufficient contrast enhancement to be detected by MRI due to assistance from the cRGD. Thus, we propose that the targeting ability of cRGD is excellent in resisting the high-shear flow conditions in large arteries.

The MRI T2-weighted images of the in vivo thrombosis before and after NP injection revealed that the Fe_3O_4-PLGA and Fe_3O_4-PLGA-cRGD NPs, with mean sizes of 289.5 and 368.2 nm and negative charges of −7.53 and −9.43 mV, respectively, were both primarily absorbed in the liver and the spleen. The NPs were internalized by specialized macrophages in the liver and the spleen within 10 min after injection. There were no significant differences in Fe_3O_4-PLGA or Fe_3O_4-PLGA-cRGD NPs uptake by each organ ($P<0.05$) at the various time points, illustrating that the conjugation of cRGD did not influence the biodistribution of the NPs. The size and surface charge clearly influenced the elimination of the NPs, with a trend consistent with the results of a previous study.[38] Although a large number of the NPs were internalized, the crucial targeting ability of Fe_3O_4-PLGA-cRGD NPs made them suitable for the detection of thrombosis. Small particles of <5 nm can pass through the glomerulus and be eliminated renally.[39] The SNRs of the kidney decreased slightly within 1 h, demonstrating that some NPs were biodegraded within an hour and cleared by the kidney.

According to a previous study,[40] iron oxide NPs possess an acceptable safety profile and are not cytotoxic at concentrations of <100 μg/mL. We administered Fe_3O_4-based NPs to rats by tail vein injection at a final dosage of 1 mg, which corresponds to an iron oxide concentration far below 100 μg/mL. This dose can thus safely achieve contrast enhancement when targeting thrombosis. The toxicokinetic properties of NPs depend on the particle type, size, surface charge, protein binding ability, exposure route, and dose, as well as on the species in question.[38] The combination of the biocompatible MR contrast agent Fe_3O_4 with a PLGA- and cRGD-based delivery system to synthesize NPs in this study did not increase toxicity. Regarding the in vivo toxicity of different NPs in rats, GPT and GOT increased slightly and temporarily within 3 h and returned to normal values after 24 h; we thus determined that, despite the large amount of uptake by the liver and spleen and some elimination by the kidneys, the Fe_3O_4-PLGA and Fe_3O_4-PLGA-cRGD NPs had no obvious effect on liver or kidney function after tail vein injection. No obvious abnormality was observed in blood composition, and no inflammatory reaction, necrosis, or abnormal cell morphology was detected in the main organs, further demonstrating that the Fe_3O_4-PLGA and Fe_3O_4-PLGA-cRGD NPs had no significant toxicity when used in vivo.

This study demonstrated the targeted enhancement of a thrombus in arteries, and based on the in vivo distribution and biological features of Fe_3O_4-PLGA-cRGD NPs, it is unclear if Fe_3O_4-PLGA-cRGD NPs can be visualized in a thrombus >1 h. Thrombus aging is a dynamic process, and time-dependent changes in thrombus composition affect thrombus stability. Future studies are needed to assess the time window of efficacy for Fe_3O_4-PLGA-cRGD NPs and their potential to discriminate between different stages of thrombus formation based on the activated platelet content. Another limitation of this study is that we did not quantify the number of NPs detected at the surface of the thrombus, under vascular endothelial cells, and in the reticular thrombus network. In future studies, we will focus on quantifying the NPs and on the penetration mechanism of Fe_3O_4-PLGA-cRGD NPs. Furthermore, as one of the most promising drug loading systems, PLGA NPs have the potential to provide effective treatment for thrombotic diseases by encapsulating certain drugs for targeted and sustained release. Our future studies will focus on the specific diagnosis and treatment of thrombosis using MRI monitoring combined with a thrombolytic drug to further investigate the complete potential of Fe_3O_4-PLGA-cRGD NPs.

Conclusion

In this study, we demonstrated the feasibility of MRI of thrombosis in vivo using novel Fe_3O_4-based PLGA NPs. Toxicity studies revealed that these NPs are sufficiently

nontoxic and biodegradable with excellent targeting ability. The NPs have good affinity for thrombi and show contrast-enhancing effects in experiments in vivo. Indeed, Fe_3O_4-PLGA-cRGD NPs represent a promising MR contrast agent for the sensitive and specific detection of thrombosis.

Acknowledgments

The authors are grateful to Yu Guo, Zhile Cao, and Jinhua Chen, MRI technologists in the Department of Radiology of Daping Hospital for their assistance with MRI technical support and *American Journal Experts* (*AJE*) for their assistance with language editing. This study was supported by the National Natural Science Foundation of China (grant nos 81171332 and 81571663).

Disclosure

The authors report no conflicts of interest in this work.

References

1. Whinna HC. Overview of murine thrombosis models. *Thromb Res*. 2008;122(Suppl 1):S64–S69.
2. Bender YY, Pfeifer A, Ebersberger HU, et al. Molecular cardiovascular magnetic resonance: current status and future prospects. *Curr Cardiol Rep*. 2016;18(5):47.
3. Previtali E, Bucciarelli P, Passamonti SM, Martinelli I. Risk factors for venous and arterial thrombosis. *Blood Transfus*. 2011;9(2):120–138.
4. Wu W, Wang Y, Shen S, et al. In vivo ultrasound molecular imaging of inflammatory thrombosis in arteries with cyclic Arg-Gly-Asp-modified microbubbles targeted to glycoprotein IIb/IIIa. *Invest Radiol*. 2013;48(11):803–812.
5. Wang X, Gkanatsas Y, Palasubramaniam J, et al. Thrombus-targeted theranostic microbubbles: a new technology towards concurrent rapid ultrasound diagnosis and bleeding-free fibrinolytic treatment of thrombosis. *Theranostics*. 2016;6(5):726–738.
6. Rix A, Fokong S, Heringer S, et al. Molecular ultrasound imaging of αvβ3-integrin expression in carotid arteries of pigs after vessel injury. *Invest Radiol*. 2016;51(12):767–775.
7. Wang X, Hagemeyer CE, Hohmann JD, et al. Novel single-chain antibody-targeted microbubbles for molecular ultrasound imaging of thrombosis: validation of a unique noninvasive method for rapid and sensitive detection of thrombi and monitoring of success or failure of thrombolysis in mice. *Circulation*. 2012;125(25):3117–3126.
8. Hu G, Liu C, Liao Y, et al. Ultrasound molecular imaging of arterial thrombi with novel microbubbles modified by cyclic RGD in vitro and in vivo. *Thromb Haemost*. 2012;107(1):172–183.
9. Bonnard T, Yang G, Petiet A, et al. Abdominal aortic aneurysms targeted by functionalized polysaccharide microparticles: a new tool for SPECT imaging. *Theranostics*. 2014;4(6):592–603.
10. Ay I, Blasi F, Rietz TA, et al. In vivo molecular imaging of thrombosis and thrombolysis using a fibrin-binding positron emission tomographic probe. *Circ Cardiovasc Imaging*. 2014;7(4):697–705.
11. Kim JY, Ryu JH, Schellingerhout D, et al. Direct imaging of cerebral thromboemboli using computed tomography and fibrin-targeted gold nanoparticles. *Theranostics*. 2015;5(10):1098–1114.
12. Suzuki M, Bachelet-Violette L, Rouzet F, et al. Ultrasmall superparamagnetic iron oxide nanoparticles coated with fucoidan for molecular MRI of intraluminal thrombus. *Nanomedicine (Lond)*. 2015;10(1):73–87.
13. von Elverfeldt D, von zur Muhlen C, Wiens K, et al. In vivo detection of activated platelets allows characterizing rupture of atherosclerotic plaques with molecular magnetic resonance imaging in mice. *PLoS One*. 2012;7(9):e45008.
14. Klink A, Lancelot E, Ballet S, et al. Magnetic resonance molecular imaging of thrombosis in an arachidonic acid mouse model using an activated platelet targeted probe. *Arterioscler Thromb Vasc Biol*. 2010;30(3):403–410.
15. McCarthy JR, Patel P, Botnaru I, Haghayeghi P, Weissleder R, Jaffer FA. Multimodal nanoagents for the detection of intravascular thrombi. *Bioconjug Chem*. 2009;20(6):1251–1255.
16. Miserus RJ, Herías MV, Prinzen L, et al. Molecular MRI of early thrombus formation using a bimodal alpha2-antiplasmin-based contrast agent. *JACC Cardiovasc Imaging*. 2009;2(8):987–996.
17. von zur Muhlen C, von Elverfeldt D, Moeller JA, et al. Magnetic resonance imaging contrast agent targeted toward activated platelets allows in vivo detection of thrombosis and monitoring of thrombolysis. *Circulation*. 2008;118(3):258–267.
18. Blasi F, Oliveira BL, Rietz TA, et al. Multisite thrombus imaging and fibrin content estimation with a single whole-body PET scan in rats. *Arterioscler Thromb Vasc Biol*. 2015;35(10):2114–2121.
19. Andia ME, Saha P, Jenkins J, et al. Fibrin-targeted magnetic resonance imaging allows in vivo quantification of thrombus fibrin content and identifies thrombi amenable for thrombolysis. *Arterioscler Thromb Vasc Biol*. 2014;34(6):1193–1198.
20. Uchiyama MK, Toma SH, Rodrigues SF, et al. Ultrasmall cationic superparamagnetic iron oxide nanoparticles as nontoxic and efficient MRI contrast agent and magnetic-targeting tool. *Int J Nanomedicine*. 2015;10:4731–4746.
21. Valdiglesias V, Fernández-Bertólez N, Kiliç G, et al. Are iron oxide nanoparticles safe? Current knowledge and future perspectives. *J Trace Elem Med Biol*. 2016;38:53–63.
22. von Zur Muhlen C, Sibson NR, Peter K, et al. A contrast agent recognizing activated platelets reveals murine cerebral malaria pathology undetectable by conventional MRI. *J Clin Invest*. 2008;118(3):1198–1207.
23. von zur Muhlen C, Peter K, Ali ZA, et al. Visualization of activated platelets by targeted magnetic resonance imaging utilizing conformation-specific antibodies against glycoprotein IIb/IIIa. *J Vasc Res*. 2009;46(1):6–14.
24. Zhang Y, Zhou J, Guo D, Ao M, Zheng Y, Wang Z. Preparation and characterization of gadolinium-loaded PLGA particles surface modified with RGDS for the detection of thrombus. *Int J Nanomedicine*. 2013;8:3745–3756.
25. Zhou J, Guo D, Zhang Y, Wu W, Ran H, Wang Z. Construction and evaluation of Fe_3O_4-based PLGA nanoparticles carrying rtPA used in the detection of thrombosis and in targeted thrombolysis. *ACS Appl Mater Interfaces*. 2014;6(8):5566–5576.
26. Chaisri W, Hennink WE, Okonogi S. Preparation and characterization of cephalexin loaded PLGA microspheres. *Curr Drug Deliv*. 2009;6(1):69–75.
27. Mao S, Xu J, Cai C, Germershaus O, Schaper A, Kissel T. Effect of WOW process parameters on morphology and burst release of FITC-dextran loaded PLGA microspheres. *Int J Pharm*. 2007;334(1–2):137–148.
28. Astete CE, Sabliov CM. Synthesis and characterization of PLGA nanoparticles. *J Biomater Sci Polym Ed*. 2006;17(3):247–289.
29. Xie S, Wang S, Zhao B, Han C, Wang M, Zhou W. Effect of PLGA as a polymeric emulsifier on preparation of hydrophilic protein-loaded solid lipid nanoparticles. *Colloids Surf B Biointerfaces*. 2008;67(2):199–204.
30. Pandita D, Kumar S, Lather V. Hybrid poly (lactic-co-glycolic acid) nanoparticles: design and delivery prospectives. *Drug Disco Today*. 2015;20(1):95–104.
31. Kapoor DN, Bhatia A, Kaur R, Sharma R, Kaur G, Dhawan S. PLGA: a unique polymer for drug delivery. *Ther Deliv*. 2015;6(1):41–58.
32. Acharya S, Sahoo SK. PLGA nanoparticles containing various anticancer agents and tumour delivery by EPR effect. *Adv Drug Deliv Rev*. 2011;63(3):170–183.

33. Dijkgraaf I, Boerman OC, Oyen WJ, Corstens FH, Gotthardt M. Development and application of peptide-based radiopharmaceuticals. *Anti Cancer Agents Med Chem*. 2007;7(5):543–551.
34. Song Y, Huang Z, Xu J, et al. Multimodal SPION-CREKA peptide based agents for molecular imaging of microthrombus in a rat myocardial ischemia-reperfusion model. *Biomaterials*. 2014;35(9):2961–2970.
35. Wen AM, Wang Y, Jiang K, et al. Shaping bio-inspired nanotechnologies to target thrombosis for dual optical-magnetic resonance imaging. *J Mater Chem B Mater Biol Med*. 2015;3(29):6037–6045.
36. Yu MK, Park J, Jon S. Targeting strategies for multifunctional nanoparticles in cancer imaging and therapy. *Theranostics*. 2012;2(1):3–44.
37. Hara T, Bhayana B, Thompson B, et al. Molecular imaging of fibrin deposition in deep vein thrombosis using fibrin-targeted near-infrared fluorescence. *JACC Cardiovasc Imaging*. 2012;5(6):607–615.
38. Lin Z, Monteiro-Riviere NA, Riviere JE. Pharmacokinetics of metallic nanoparticles. *Wiley Interdiscip Rev Nanomed Nanobiotechnol*. 2015;7(2):189–217.
39. Ittrich H, Peldschus K, Raabe N, Kaul M, Adam G. Superparamagnetic iron oxide nanoparticles in biomedicine: applications and developments in diagnostics and therapy. *Rofo*. 2013;185(12):1149–1166.
40. Laurent S, Saei AA, Behzadi S, Panahifar A, Mahmoudi M. Superparamagnetic iron oxide nanoparticles for delivery of therapeutic agents: opportunities and challenges. *Expert Opin Drug Deliv*. 2014;11(9):1449–1470.